arXiv:astro-ph/9802353v1 27 Feb 1998

Model Photospheres for Late-Type Stars from the Inversion of High-Resolution Spectroscopic Observations. The Sun

Carlos Allende Prieto, Basilio Ruiz Cobo, and Ramón J. García López

Instituto de Astrofísica de Canarias,

E-38200 La Laguna, Tenerife,

Spain

Received _____; accepted _____

ABSTRACT

An inversion technique has been developed to recover LTE one-dimensional model photospheres for late-type stars from very high resolution, high signal-to-noise stellar line profiles. It is successfully applied to the Sun by using a set of clean Ti I, Ca I, Cr I, and Fe I normalized line profiles with accurate transition probabilities and taking advantage of the well understood collisional enhancement of the wings of the Ca I line at 6162 Å. Line and continuum center-to-limb variations, continuum flux, and wings of strong metal lines are synthesized by means of the model obtained and are compared with solar observations, as well as with predictions from other well known theoretical and empirical solar models, showing the reliability of the inversion procedure. The prospects for and limitations of the application of this method to other late-type stars are discussed.

Subject headings: line: profiles – radiative transfer – Sun: photosphere – stars: atmospheres – stars: late-type

1. Introduction

Model photospheres for late-type stars are a fundamental cornerstone of modern Astronomy. The Sun, our closest star, belongs to this stellar category and its atmosphere provides an exceptional plasma laboratory to study detailed physical processes. Late-type stars are also the most numerous group in the Galaxy. They not only dominate its present dynamics, but their photospheric abundances constitute a unique tool for tracing its chemical evolution history. Furthermore, the oldest unevolved stars in the Galaxy, which provide information about the physical conditions at early epochs and constraints on models of primordial nucleosynthesis, are also late-type stars.

In this century, considerable efforts have been devoted to theoretical and empirical modeling of late-type stellar atmospheres. In this respect, particular success was achieved in the seventies, and most of the models used nowadays are mainly based on work carried out in that decade. For a comprehensive review of the state of the art in the modeling of photospheres of F- and later-type stars see, for example, the discussion by Gustafsson & Jørgensen (1994) and Avrett (1996). Classical theoretical models are usually computed under the simplifying assumptions of hydrostatic equilibrium, plane-parallel stratification, local thermodynamic equilibrium (LTE), and conservation of energy flux (treating convection with the mixing length approximation). High-resolution, high signal-to-noise ratio spectra over extensive spectral ranges can be used to test the validity of existing theoretical models and to better constrain the observational features which have to be reproduced (line profiles and asymmetries, excitation and ionization equilibria of different elements, stellar fluxes, etc.).

These data can also be used to construct models by using observed features to find a temperature–depth ($T-\tau$) relation. Semi-empirical models of this kind have been obtained for the solar photosphere, where the present-day knowledge of the abundances of different

elements, as well as its extended disk, allow a better observational constraint. The model constructed by Holweger & Müller (1974) is a good example of this class and has been widely used not only for the Sun but also for other late-type stars by scaling its $T - \tau$ relation to different stellar effective temperatures. Although the spatially resolved information that can be obtained for the Sun is lacking for other late-type stars, spectral lines do contain enough information to determine reliable values for the physical magnitudes governing the state of a stellar atmosphere, and this approach has been applied, for instance, to the modelling of giant stars such as Arcturus (Mäckle et al. 1975) and Pollux (Ruland et al. 1980).

The so-called spectroscopic *inversion* methods are aimed at obtaining the model atmosphere from which the synthetic line profiles best match the observed ones (usually with a least-squares criterion). The availability of high-quality data (observed spectra and line parameters) and modern computers make possible these inversions by taking into account the information contained in the whole line profile, which can potentially provide not only the temperature stratification in the atmosphere but also insights into other physical magnitudes such as velocity and magnetic fields.

This paper is part of a wider project aimed at better understanding the photospheres of late-type stars of different metallicities for use in studies of Galactic chemical evolution and primordial nucleosynthesis. Among the different approaches envisaged within this project, which incorporates the study of theoretical model atmospheres and the presence and extension of line asymmetries in the photospheres of metal-poor stars, we present here a successful attempt to obtain a semi-empirical solar model photosphere by inverting observed clean line profiles with accurate oscillator strengths. This kind of information is also available for other late-type stars (with different levels of metallicity), and what we learn from modeling the Sun will help us when trying to apply the method to other stars. Section 2 provides the details of the inversion code, which is based on a well-tested inversion method for the

Stokes parameter vector; §3 shows its application to the solar case and the comparison of its results with those associated with other well-known theoretical and semi-empirical models. We describe in §4 the potential use and limitations in applying the code to other late-type stars, and the main conclusions and the perspectives for the near future are summarized in §5.

2. The inversion code

The MISS (Multiline Inversion of Stellar Spectra) code described in this paper is an adaptation of a previous inversion method of Stokes vector spectra: the SIR method (Ruiz Cobo & del Toro Iniesta 1992; see also del Toro Iniesta & Ruiz Cobo 1995, 1996, 1997). The SIR code has recently been applied to the study of different solar structures observed in polarized light, such as sunspots (Collados et al. 1994; Westendorp Plaza et al. 1997a,b,c), and unresolved magnetic elements in facular regions (Bellot Rubio, Ruiz Cobo & Collados 1997), and for non-polarized light to structures such as penumbrae (del Toro Iniesta, Tarbell & Ruiz Cobo 1994), solar granulation (Ruiz Cobo et al. 1995, 1996; Rodríguez Hidalgo, Ruiz Cobo & Collados 1996), and the solar 5-min oscillation (Rodríguez Hidalgo, Ruiz Cobo & Collados 1997; Ruiz Cobo, Rodríguez Hidalgo & Collados 1997). A study of its performance versus other inversion techniques can be found in Wood & Fox (1995) and Westendorp Plaza et al. (1998).

Our inversion method iteratively modifies an initial model atmosphere until an optimal fit of the observed profiles is reached. The model atmosphere contains a set of values of temperature, microturbulence, and line-of-sight velocity evaluated on an equally spaced logarithmic scale of the optical depth of the continuum at 5000 Å (τ_{5000}), together with a set of optical depth-independent parameters such as rotation velocity ($v \sin \hat{\imath}$), macroturbulent velocity amplitude, and chemical abundances. Gravity is fixed and the gas and electronic

pressures are computed to satisfy hydrostatic equilibrium, the ideal gas equation of state, and the Saha equation.

In this section we will pay special attention to the differential features between our inversion code (MISS) and the progenitor (SIR), describing its particularities within three subsections dedicated to hypotheses and model parameterization, spectral synthesis, and inversion algorithm.

2.1. Hypotheses and model parameterization

In order to simplify the synthesis process, as well as to keep the number of free parameters small enough, a set of hypotheses has been assumed: the LTE approximation, a steady-state, plane-parallel, one-dimensional atmosphere, solid body rotation, hydrostatic equilibrium, radial bulk velocity, and negligible magnetic field.

To evaluate the continuum absorption coefficient, contributions from H, He, H^-, He^-, H_2^-, H_2^+, C, Mg, Na, and scattering terms have been taken into account. Other atomic and molecular line opacity sources, which are neglected here, can also be included.

To obtain an accurate solution of the transfer equation the number of points (optical depth values) through the atmosphere has to be about 50. Considering the values for every one of the depth-dependent quantities as free parameters would imply solving a system of more than 150 dimensions. To simplify the numerical problem, following the SIR strategy, the perturbations of depth-dependent quantities are evaluated only in a discrete number of points in τ_{5000}, called *nodes*. The entire stratifications of the various parameters are thus obtained by adding the result of a spline interpolation of the perturbations at the nodes to the initial stratification. For each parameter a different number of nodes can be selected by the user. Experience from the quoted applications of SIR reveals that the optimum solution

is reached by steadily increasing the degree of complexity of perturbations (i.e., the number of nodes) from one iteration to the next, until no significant improvement in the fit between the observed and synthesized profiles is reached.

Provided the quantity and quality of observational data allow a corresponding increase in the number of free parameters, some of the previous hypotheses can be relaxed in the framework of the present MISS code: the homogeneous atmosphere can be substituted for a two-component atmosphere in order to take the effect of convective motions into account; the hydrostatic-equilibrium hypothesis can be ignored by considering the electron-pressure stratification as a free parameter; the application of MISS to the determination of magnetic fields is straightforward, since this code is a simplified version of SIR, a procedure for Stokes vector inversion. Nevertheless, as will be shown below, the amount of information we shall be able to extract is strongly limited by problems deriving from the accuracy of atomic parameters (mainly oscillator strengths), as well as from the presence of observational noise. Therefore, up to the present time, the search for inhomogeneous, magnetized or far from hydrostatic equilibrium models is beyond our reach. Concerning the LTE approach, a project is at present in progress for inversion of the Stokes parameter vector under the following hypotheses: a steady-state atmosphere, complete redistribution on scattering, LS-coupling, and no quantum interference between Zeeman states (Socas-Navarro et al. 1996, Socas-Navarro, Ruiz Cobo & Trujillo Bueno 1998).

2.2. Spectral synthesis

A typical application of MISS to spectroscopic observations implies the solution of the radiative transfer equation a large number of times. There are several reasons for this: the inversion problem must be solved iteratively due to the non-linear dependence of the spectral profiles on the physical quantities; to evaluate the stellar flux, the solution of the radiation

transfer equation must be calculated for several lines of sight; and finally many spectral lines are needed to obtain a reliable model. Therefore, spectral synthesis is the most time-consuming part of the code, and it is of paramount importance to have a fast integration method. MISS uses a new one, recently developed by Bellot Rubio, Ruiz Cobo & Collados (1998), which is based on the Taylor expansion of the Stokes parameter vector (only the specific intensity in our case) to fourth order in depth. Compared to other methods, the new technique turns out to be superior in terms of speed and accuracy. It also gives an approximation to response functions (RFs, the derivatives of specific intensity with respect to the perturbation of each free parameter; see Ruiz Cobo & del Toro Iniesta 1992, 1994), which are a fundamental ingredient of the inversion algorithm.

The following quadrature has been used to evaluate the energy flux, F, at a given wavelength, λ, from the specific intensity, I, computed at each point μ across the stellar disk:

$$F(\lambda) = \int_0^1 \mu\, I(\lambda,\mu)\, \mathrm{d}\mu \approx \sum_i^n w_i\, I(\lambda,\mu_i), \tag{1}$$

where μ_i are the abscissae and w_i are the weighting factors for Gaussian integration. Using solar model atmospheres from the literature, it has been numerically checked that a quadrature of order $n \approx 5$ is enough to guarantee that the integration precision exceeds the observational data accuracy.

When taking into account the influence of the instrumental profile, $P(\lambda)$, macroturbulence, $M(\lambda)$, and rotation, $G_i(\lambda)$, for the i-th annulus (see Appendix A for details), equation (1) becomes:

$$F(\lambda) = \left[\sum_i^n w_i\, I(\lambda,\mu_i) * G_i(\lambda)\right] * P(\lambda) * M(\lambda), \tag{2}$$

where "$*$" means convolution. The instrumental profile, including telescope and spectrograph, can be provided either as input or approximated by a Gaussian in which σ depends on the spectral resolution. The macroturbulence profile is a Gaussian with σ proportional to the amplitude of the macroturbulent velocity.

2.3. Inversion algorithm

The algorithm is the same as used by SIR, and a detailed description of it can be found in the above mentioned references. A brief overview is presented below.

Inversion of observed data is performed by using a non-linear least-squares algorithm which involves the minimization of a merit function:

$$\chi^2 \equiv \frac{1}{\nu} \sum_{i=1}^{i=M} [F^{\rm obs}(\lambda_i) - F^{\rm syn}(\lambda_i)]^2, \tag{3}$$

where index $i = 1, 2, \ldots, M$ stands for the wavelength samples, indices "obs" and "syn" refer to observed and synthetic data, respectively, and ν is the number of degrees of freedom.

Minimization of the merit function is carried out through a Marquardt algorithm (Marquardt 1963), modified by applying a singular value decomposition (SVD; Press et al 1986). This algorithm requires the evaluation of the derivatives of χ^2 with respect to each free parameter. These derivatives can be directly expressed in terms of response functions, which are calculated by applying a quadrature (eq. [1]) to the RF of the specific intensity provided by the integration method. Elimination of singularities (via SVD in this case) is essential because certain free parameters (e.g., temperature in layers where the line profile has no sensitivity) may produce a null effect on the emergent flux and consequently make the problem undetermined.

To summarize, the steps of the procedure are:

1. Choice of a guess model and a number of nodes for each free parameter.

2. Calculation of flux, RF, and χ^2.

3. Iterative evaluation of a new model after application of the Marquardt algorithm, until minimization of χ^2 is reached.

4. Subsequent modification of the number of nodes and iteration from step 2 until χ^2 ceases to decrease significantly.

3. Application of the method: The Sun

The SIR method has been successfully applied to the Sun taking advantage of its spatially resolved disk and the high quality of solar observations (see references in §2). The Sun is also the best known late-type star and provides a unique opportunity to field-test the potential of the MISS technique for the Sun seen as a star.

3.1. Input data

The widely used high-resolution Solar Flux Atlas of Kurucz et al. (1984) was selected as the source of the line profiles. Its complete spectral coverage in the 2960–130000 Å region, with a very high signal-to-noise ratio ($\sim$ 2500), and the extremely high spectral resolution ($\lambda/\Delta\lambda \sim 400000$) makes it ideal for our purposes. Furthermore, Allende Prieto & García López (1998) have recently verified the reliability of the wavelength calibration of this atlas by measuring the central wavelength shifts of 1446 Fe I lines with accurate laboratory determinations.

It was required that the input lines to be included in the inversion be selected from the compilation of solar lines by Meylan et al. (1993), who identified clean line wings in the same atlas by fitting Voigt profiles. We also impose the condition that the atomic transition probability had been measured at the Oxford furnace (see, e.g., Blackwell & Shallis 1979). Their oscillator strengths ($\log gf$) are usually recognized as the most accurate ones present in the literature. Several tests were carried out to study the dependence of the method on the accuracy of the oscillator strengths used. It turned out that when artificially introducing errors in the $\log gf$ values larger than $\sim$ 5 % the inversion returns errors larger than 2% in the temperature stratification. Furthermore, special attention was given to the chemical elements selected. We mainly focused on lines of elements which show an agreement between their photospheric and meteoritic abundances, as it is more likely for the abundance errors to be smaller. Although iron does not satisfy this condition, it was felt that the significant increase in the number of useful lines justified its inclusion. Finally, in an effort to minimize the problems related to the lack of knowledge of the collisional damping of the lines, features stronger that 80 mÅ (equivalent width) were rejected.

The method is able to extract information only on the photospheric region corresponding to the depth range where the employed lines are formed. To improve the sampling of the photospheric domain, whole line profiles or just single wings were accepted as input data following the considerations of the line cleanness by Meylan et al. (1993).

A total of 40 absorption lines produced by neutral iron, titanium, chromium and calcium entered the inversion program. The wings of the stronger Ca I λ 6162 Å were included with the aim of extending the depth coverage. This is one of the few spectral lines for which the collisional enhancement of the wings is well known (see Allende Prieto, García López & Trujillo Bueno 1997), there being a reasonable agreement between theoretical analyses and semi-empirical measurements. This consideration is mandatory in order to wide the input

information without introducing new uncertainties. The collisional width of the line was interpreted in terms of collisions with neutral hydrogen, as computed by Spielfiedel et al. (1991). Table 1 lists the lines entering the inversion and their parameters.

An attempt was made to employ the spectral information contained in both the continuum and the line shapes. The observed continuum may differ strongly from the true one in the blue ($\lambda < 5000$ Å) due to the line absorption, so we can determine only a lower limit for the flux at these wavelengths. Even the measurement of the pseudo-continuum is a non-trivial matter: the discrepancies among different authors are as high as 8% (see, e.g., Burlov-Vasiljev, Gurtovenko & Matvejev 1995). The slope of the continuum is closely linked to the temperature gradient in the photosphere in such a way that the employment of the information stored in the continuum requires highly accurate spectrophotometry. This led us to exclude the absolute calibration of the line profiles entering the inversion code, and only line profiles normalized to their local continuum were used.

3.2. Procedure

Starting from an isothermal model photosphere, step by step the depth dependence of the temperature is allowed to be modified in a successively increasing number of nodes. No vertical velocity gradient was allowed for, and the microturbulence was assumed to be constant with depth. A Gaussian profile was employed to represent the instrumental profile. Three snapshots of the inversion process are shown in Fig. 1 (ordered a, b, and c). The evolution of the synthetic profiles for several of the lines included in the inversion is shown and compared with the solar observations (dots). A constant-temperature model photosphere (dotted line) does not produce any line absorption, while the final model (solid line) provides lines which get very close to the observed features. Starting from the solar abundances listed by Anders & Grevesse (1989), the successive modification of the abundance of the considered

elements was allowed for, providing an excellent final fit. This resulted in no variation of any of the abundances except for iron, which dropped from the initial value log N(Fe) = 7.67 to 7.48 (where log N(H) = 12), very close to the meteoritic abundance. Using the synodic equatorial velocity of 1.88 km s^{-1} and the microturbulence of 0.6 km s^{-1} (consistent with Takeda 1995), the code arrives at 1.7 km s^{-1} for the macroturbulent velocity.

As an example, one of the lines employed in the inversion procedure is displayed in more detail in Fig. 2, comparing the final synthetic profile (solid line) with the solar feature (circles). The point has been reached where no closer fit is possible without taking the line asymmetries into account. The observed asymmetries have their origin mainly in the correlation between temperature and convective velocities, as observed in the solar granulation, although blends, isotopic or hyperfine splitting might be responsible for particular cases (Gray 1980; Dravins, Lindegren & Nordlund 1981; Kurucz 1993). A more complex treatment than a plane-parallel one-dimensional static single-component model photosphere is required to reproduce it (e.g., Dravins & Nordlund 1990a,b; Rast et al. 1993).

Figure 3 shows the final model photosphere, which we will refer to as MISS hereafter, compared with other well-known models from the literature: Kurucz (1992), Holweger & Müller (1974; hereafter HOLMU), Vernazza, Avrett & Loeser (1981; hereafter VALC), and Gingerich et al. (1971; Harvard Smithsonian Reference Atmosphere, hereafter HSRA). Kurucz's model is based on theoretical calculations assuming LTE, hydrostatic equilibrium and taking the line blanketing into account. The model of Howeger & Müller was empirically adjusted to reproduce continuum observations in the optical and near infrared, as well as equivalent widths and residual intensities of Fe I spectral lines. The VALC empirical model was based on observations of the ultraviolet continuum, taking into account the departures from LTE. And HSRA was basically designed to reproduce observations of the solar continuum.

The error bars shown for the MISS model have been computed following the recipe described in Ruiz Cobo et al. (1997) and limit the depth range where the lines employed sample the atmosphere; that is, where the model is meaningful. The MISS model shows, in general, a very similar temperature dependence to that of the other models, tending to be cooler in the upper part of the photosphere and hotter in the inner part.

3.3. Properties of the model derived

Insight into the quality of the model photosphere obtained can be achieved by comparing the behavior of predicted and observed features not included in the empirical modeling. Choosing what we consider as the most significant features, systematic comparisons with other well-established model photospheres for the Sun are shown below.

3.3.1. Limb darkening

The center-to-limb variation observed in the Sun maps the temperature stratification of the solar photosphere and hence is probably one of the best tools for testing a one-dimensional model photosphere. Figure 4 shows the comparison at $\lambda\lambda$ 3500, 4163, 4774, 5799, 7487, and 10990 Å between polynomial fits to the continuum observations of Neckel & Labs (1994) and the predictions from the different models considered. The difference between the observed and computed intensities against μ (the cosine of the position angle on the solar surface with respect to our line of sight) is plotted, normalized to their corresponding values at the disk center. HOLMU reproduces in detail the observed variation at $\sim$ 1 μm, the agreement being worse at shorter wavelengths. To make a fully legitimate comparison at short optical wavelengths ($\lambda < 5000$ Å), it will be necessary to clarify first whether or not the thousands of lines in the blue part of the optical spectrum do seriously change the observed

limb-darkening from its shape in the true continuum. HSRA provides the best general comparison at all wavelengths, while the limb-darkening predicted by the MISS model keeps close to the observations for the whole optical range.

There are observations available for the variation of line profiles across the disk. Balthasar (1988) lists the center-to-limb variation for the equivalent widths of 143 lines, and shows that the behavior of the different lines is not homogeneous. A comparison between the observations and predictions from the model atmospheres is shown in Figure 5. The variation of the equivalent widths normalized to the center of the disk is shown for three lines in common between our line list and Balthasar's measurements. It can be seen how the absolute synthetic equivalent widths (with values in the range 70–100 mÅ) are underestimated with respect to the observed ones, arising from the use of the Van der Waals approach for the collisional enhancement of the line wings. Although the chemical abundances of the different elements are able to alter the curves, and the temperature dependence of the collisional width is more likely to be $T^{0.4}$, rather than the Van der Waals dependence of $T^{0.3}$ (e.g., Allende Prieto et al. 1997), we deduce from the figure that the model obtained from the inversion behaves remarkably better than the others. Caution must be taken regarding the HSRA and VALC models: both were constructed under NLTE and the synthetic profiles shown here were calculated under LTE. A more precise way of carrying out this comparison would be to use directly the wing profiles of lines with accurate broadening parameters, such as the sodium D lines and the Ca I $4s4p$–$4s5s$ lines at $\lambda\lambda$ 6102.72, 6122.22, and 6162.17 Å.

3.3.2. Continuum flux

As previously noted, although there is some disagreement in the literature, the absolute solar flux can be used as a lower limit for the true continuum. This may help to discard model atmospheres predicting lower true continuum fluxes than the measured pseudo-continuum.

Figure 6 shows the comparison between the measurements by Neckel & Labs (1984; triangles), the pseudo-continuum estimated from the correction of the line absorption observed in the high-resolution solar spectrum of Kurucz et al. (1984; dots), and the theoretical true continua as predicted by several classical solar models. Kurucz (1992) claims that his solar model reproduces the solar observations of Neckel & Labs (1984) with high accuracy and, according to this, the true continuum calculated by taking no line absorption into account is well over the pseudo-continuum. That is not the case for the continua associated with two of the empirical models, HSRA and VALC, being the continuum predicted by HOLMU higher than the pseudo-continuum but not as much as Kurucz's model.

The model we obtained from only the inversion of line profiles gives rise to a continuum very similar (somewhat brighter) to that from the theoretical model by Kurucz. This is a remarkable property, because the MISS model was constructed from line profiles normalized to the local continuum without considering any data on the absolute flux at any wavelength or any other photometric information.

3.3.3. Strong features

The Ca I λ 6162.17 Å line was already included in the inversion procedure and its synthetic profile obtained using the MISS model provides an excellent fit to the observed solar atlas, as can be seen in the upper panel of Figure 7. This is also the case for the other two Ca I lines corresponding to the $4s4p$–$4s5s$ multiplet. It is also worthwhile noting the remarkably good fit obtained for other lines surrounding the λ 6162.17 Å line, not considered in the inversion, for which no necessarily high-quality[1] transition probabilities

[1]The Vienna Atomic Line Database (VALD) provided us with the transition probabilities, except for Ca I $\lambda\lambda$ 6161 and 6162 Å lines

have been used.

Another important comparison associated with strong features is shown in the lower panel of Figure 7. The predicted wings of the sodium D doublet, which are supposed to cover a wide depth range of the photosphere and be formed under the LTE approximation (Covino et al. 1993), nicely reproduce the observed solar profiles.

3.3.4. Weak lines not included in the inversion

Apart from the lines included in the inversion, it is of great interest to compare predicted and observed profiles of other lines for which accurate transition probabilities are available. A very suitable group of lines for this purpose are the Fe I lines measured by O'Brian et al. (1991) with an accuracy better than 5 %, which belong to the Meylan et al. (1993) selection, but are not included in the Oxford line lists. Figure 8 shows this comparison for three Fe I lines located at $\lambda\lambda$ 4635.85, 6027.05, and 6481.87 Å. We have assumed an iron abundance of log N(Fe)= 7.48, a macroturbulent velocity of 1.7 km s^{-1} (the values obtained from the inversion), and a constant microturbulence of 0.6 km s^{-1}. The profiles were computed in LTE in all cases. It can be seen that the best fits correspond to MISS, followed very closely by VALC, and then by HSRA (although these are NLTE models), Kurucz, and HOLMU, respectively.

It can be concluded then that the MISS model reproduces, in general, several key observational constraints with a quality similar to that of other well-known models and behaves better than several of these models when focusing on particular comparisons.

4. Application to other late-type stars

As explained in the introduction, the final goal of this work is to develop a spectroscopic tool for deriving semi-empirical model photospheres for late-type stars in general, and for metal-poor stars in particular. In principle, the information used here for the solar case (normalized line profiles with very high resolution and high signal-to-noise ratio) can be also available for other bright stars. Allende Prieto et al. (1995) have shown preliminary observations of a metal-poor star obtained with $R \equiv \lambda/\Delta\lambda \sim 170000$ and S/N$\sim$ 300–600. Observations of the same and other stars with slightly higher resolution and better signal-to-noise ratios have been already carried out and are being processed. These values of R and S/N are, however, significantly smaller than those associated with the solar atlas we have used. Furthermore, the wavelength coverage achieved in the stellar observations is much smaller than that available for the Sun. It will be necessary then to test in detail what happens in the inversion when using different numbers of lines combined with spectra of lower quality. This is, in any case, a practical problem which can be solved by using ultra-high resolution spectrographs to observe very bright objects.

A different problem associated with this semi-empirical procedure is related to the spectral synthesis itself in terms of knowledge of the atomic and molecular opacities (especially for metal-poor stars), effects of non-LTE, convection and overshooting, etc. A way for partially minimizing these effects would be to use as many lines as possible with accurate transition probabilities and damping constants, and also to focus as much as possible on near-infrared lines where the opacity problems decrease.

5. Conclusions

The Multiline Inversion of Stellar Spectra (MISS) procedure developed here has been proved able to find an LTE temperature stratification for the solar photosphere from normalized high-resolution line profiles which reproduces the solar continuum and the limb-darkening sufficiently well and is in excellent agreement with observed strong and weak spectral lines with accurate line data. A better comparison of its performance in reproducing the limb-darkening of the wings of strong lines with accurate damping constants is now being studied.

It is found that none of the input abundances (Anders & Grevesse 1989) for chromium, calcium, and titanium need to be changed to find the best fit to the observations, but the iron abundance is preferred to vary from the initially assumed value (7.67, in the scale where the hydrogen abundance is 12) to the lower (approximately meteoritic) abundance 7.48.

A better fit to the solar flux line spectrum would require the abandonment of the hypothesis of hydrostatic equilibrium and the introduction of multi-component models or velocity fields inducing asymmetries in the line profiles. Our work in the near future will consider this improvement.

This procedure of semi-empirical modeling of stellar photospheres can potentially be applied to other late-type stars. While other classical methods of empirical modeling would require observations not available for stars (the limb-darkening cannot be measured yet, and flux calibrated spectra are affected by a number of larger uncertainties), the normalized line profiles used by MISS are already at hand.

We express our gratitude to L. R. Bellot Rubio, M. Collados, E. Simmoneau, and J. C. del Toro Iniesta for interesting comments on the draft. We also thank T. Meylan, who kindly provided a digital version of his line list. This article has been corrected for English

and style by Terry Mahoney (Research Division, IAC). NOS/Kitt Peak FTS data used here were produced by NSF/NOAO. This research has made use of the VALD database and was partially supported by the Spanish DGES under projects PB95-1132-C02-01 and PB95-0028.

A. Evaluation of the rotation profile

The effect of the rotation on the spectral profile has been estimated by taking advantage of the knowledge of the specific intensity of the local continuum for each spectral line $I_c(\lambda, \mu_i), \quad i = 1, \cdots, n$, where n is the number of points of the quadrature used. Let $r_{\mu_i} = \sqrt{1-\mu_i^2}, \quad i = 1, \cdots, n$ be the normalized radius corresponding to the point with cosine of the heliocentric angle μ_i. The stellar disk is considered divided into n annuli with internal and external radii r_i and R_i, respectively, defined as follows: $r_1 = 0$, $r_i = (r_{\mu_{i-1}} + r_{\mu_i})/2, \;\; i = 2, \cdots, n$, $R_i = r_{i+1}, \;\; i = 1, \cdots, n-1$, and $R_n = 1$. Let us assume that $I_c(\lambda, \mu)$ varies linearly between μ_i and μ_{i+1}, in the following way:

$$\begin{aligned} I_c(\lambda,\mu) &= a_i\ \mu + b_i, \quad \text{with} \quad \mu_{i-1} \geq \mu \geq \mu_{i+1}, \;\; i = 2, \cdots, n-1 \\ I_c(\lambda,\mu) &= a_2\ \mu + b_2, \quad \text{with} \quad \mu \geq \mu_1 \\ I_c(\lambda,\mu) &= a_{n-1}\ \mu + b_{n-1}, \quad \text{with} \quad \mu \leq \mu_n \end{aligned} \tag{A1}$$

The line-of-sight component of the rotation velocity will be the same for all points located at an equal distance x from the central meridian: $v_x = v \sin \hat{\imath}\ x$. The flux crossing the fraction of area of the i-th annulus at a distance between x and $x + \mathrm{d}x$ is given by

$$F_{x,i} = a_i \ \Big[y_i\ \mu_{r_i} - y_{i-1}\ \mu_{r_{i-1}} + (1-x^2)\ (\theta_i - \theta_{i-1}) \Big] + 2\ b_i (y_i - y_{i-1}), \tag{A2}$$

for $i = 1, \cdots, n$, where $\mu_{r_i} = \sqrt{1 - {r_i}^2}$, $\mu_{r_0} = 0$, $\theta_i = \arcsin(\frac{y_i}{\sqrt{1-x^2}})$, and $y_i = \sqrt{r_i^2 - x^2}$. From these expressions the rotation profile for each annulus can be written as

$$G_i = \frac{F_{x,i}\ c}{\lambda_0\ v \sin \hat{\imath}\ x\ \int_{r_i}^{R_i} F_{x,i}\ \mathrm{d}x}. \tag{A3}$$

REFERENCES

Allende Prieto, C., & García López, R. J. 1998, A&AS (in press)

Allende Prieto, C., García López, R. J., Lambert, D. L., & Gustafsson, B. 1995, in IAU Symp. 176, Stellar Surface Structure, Poster Proceedings, ed. K. G. Strassmeier (Vienna: Institut für Astronomie der Universität Wien), 107

Allende Prieto, C., García López, R. J., & Trujillo Bueno, J. 1997, ApJ, 483, 941

Anders, E., Grevesse, N. 1989, Geochimica et Cosmochimica Acta, 53, 197

Avrett, E. 1996, in IAU Symp. 176, Stellar Surface Structure, ed. K. G. Strassmeier & J. L. Linsky (Dordrecht: Kluwer), 503

Balthasar, H. 1988, A&AS, 72, 473

Bellot Rubio L. R., Ruiz Cobo B., & Collados M. 1997, ApJ, 478, L45

Bellot Rubio L. R., Ruiz Cobo B., & Collados M. 1998, ApJ (submitted)

Blackwell, D. E., & Shallis, M. J 1979, MNRAS, 186, 669

Burlov-Vasiljev, K. A. Gurtovenko, E. A., Matvejev, Yu. B. 1995, Solar Phys., 157, 51

Collados, M., Martínez Pillet, V., Ruiz Cobo, B., del Toro Iniesta, J.C., & Vázquez, M. 1994, A&A, 291, 622

Covino, E., Gomez, M. T., Severino, G., & Franchini, M. 1993, in ASP Conf. Series, vol. 40, Inside the Stars, eds. W. W. Weiss & A. Baglin (San Francisco: ASP), 190

Dravins, D., Lindegren, L., & Nordlund, Å. 1981, A&A, 96, 345

Dravins, D., & Nordlund, Å 1990a, A&A, 228, 184

Dravins, D., & Nordlund, Å 1990b, A&A, 228, 203

Gingerich, O., Noyes, R. W., Kalkofen, W., & Cuny, Y., 1971, Solar Phys., 18, 347

Gray, D. F. 1980, ApJ, 235, 508

Gustafsson, B., & Jørgensen, U. G. 1994, A&A Rev., 6, 19

Holweger, H., & Müller, E. A. 1974, Solar Phys., 39, 19

Kurucz, R. L. 1992, in IAU Symp. 149, The Stellar Populations of Galaxies, ed. B. Barbuy & A. Renzini (Dordrecht: Kluwer), 225

Kurucz, R. L. 1993, Physica Scripta, T47, 110

Kurucz, R. L., Furenlid, I., Brault, J., & Testerman, L. 1984, NOAO Atlas No. 1, The Solar Flux Atlas from 296 to 1300 nm (Sunspot, NM: National Solar Observatory)

Marquardt, D. W. 1963, J. Soc. Ind. Appl. Math., 11, 431

Mäckle, R., Holweger, H, Griffin, R., & Griffin, R. 1975, A&A, 38, 239

Meylan, T., Furenlid, I., Wiggs, M. S., Kurucz, R. L. 1993, ApJS, 85, 163

Neckel, H., & Labs, D. 1984, Solar Phys., 90, 205

Neckel, H., & Labs, D. 1994, Solar Phys., 153, 91

O'Brian, T. R., Wickliffe, M. E., Lawler, J. E., Whaling, W., & Brault, J. W. 1991, J. Opt. Soc. Am. B, 8, 1185

Press, W. H., Flannery, B. P., Teukolsky, S. A., & Vetterling, W. T. 1986, Numerical Recipes (Cambridge: Cambridge University Press)

Rast, M. P., Nordlund, Å, Stein, R., & Toomre, J. 1993, ApJ, 408, L53

Rodríguez Hidalgo, I., Ruiz Cobo, B., & Collados, M. 1996, in ASP Conf. Ser. 109, Cool Stars, Stellar Systems, and the Sun, 9$^{\rm th}$ Cambridge Workshop, ed. R. Pallavicini, & A. K. Dupree (San Francisco: ASP), 155

Rodríguez Hidalgo, I., Ruiz Cobo, B., & Collados, M. 1997, Solar Phys., 172, 72

Ruiz Cobo, B., Rodríguez Hidalgo, I., & Collados, M. 1997, ApJ, 488, 462

Ruiz Cobo, B., & del Toro Iniesta, J. C. 1992, ApJ, 398, 375

Ruiz Cobo, B., & del Toro Iniesta, J. C. 1994, A&A, 283, 129

Ruiz Cobo, B., del Toro Iniesta, J. C., Rodríguez Hidalgo, I., Collados, M., & Sánchez Almeida, J. 1995, JOSO Annual Report, 162

Ruiz Cobo, B., del Toro Iniesta, J. C., Rodríguez Hidalgo, I., Collados, M., & Sánchez Almeida, J. 1996, in ASP Conf. Ser. 109, Cool Stars, Stellar Systems, and the Sun, 9th Cambridge Workshop ASP Conference, eds. R. Pallavicini & A.K. Dupree (San Francisco: ASP), 155

Ruland, F., Holweger, H., Griffin, R., Griffin, R., & Biehl, D. 1980, A&A, 92, 70

Socas-Navarro, H., Trujillo Bueno, J., Ruiz Cobo, B., & Shchukina, N. G. 1996, JOSO Annual Report, 86

Socas-Navarro, H., Ruiz Cobo, B., & Trujillo Bueno, J. 1998, ApJ (in preparation)

Spielfiedel, A., Feautrier, N., Chambaud, G., & Lévy, B. 1991, J. Phys. B, 24, 4711

Takeda, Y. 1995, PASP, 47, 337

del Toro Iniesta, J. C., & Ruiz Cobo, B. 1995, in La polarimétrie, outil pour l'étude de l'activité magnétique solaire et stellaire, eds. N. Mein & S. Sahal-Bréchot (Paris: Observatoire de Paris-Meudon), 127

del Toro Iniesta, J. C., & Ruiz Cobo, B. 1996, Solar Phys., 164, 169

del Toro Iniesta, J.C., & Ruiz Cobo, B. 1997, in Forum THEMIS, Observatoire de Paris-Meudon, eds. N. Mein & S. Sahal-Bréchot (Paris: Observatoire de Paris-Meudon), 93

del Toro Iniesta, J. C., Tarbell T. D., & Ruiz Cobo, B. 1994, ApJ, 436, 400

Vernazza, J. E., Avrett, E. H., & Loeser, R. 1981, ApJS, 45, 635

Westendorp Plaza, C., del Toro Iniesta, J. C., Ruiz Cobo, B., Martínez Pillet, V., Lites, B. W., & Skumanich, A. 1997a, in 1st Advances in Solar Physics Euroconference.

Advances in the Physics of Sunspots, eds. B. Schmieder, J. C. del Toro Iniesta, & M. Vázquez, ASP Conf. Ser. Vol. 118, 197

Westendorp Plaza, C., del Toro Iniesta J. C., Ruiz Cobo, B., Martínez Pillet, V., Lites, B. W., & Skumanich, A. 1997b, in 1st Advances in Solar Physics Euroconference. Advances in the Physics of Sunspots, eds. B. Schmieder, J.C. del Toro Iniesta, & M. Vázquez, ASP Conf. Ser. Vol. 118, 202

Westendorp Plaza, C., del Toro Iniesta, J. C., Ruiz Cobo, B., Martínez Pillet, V., Lites, B. W., & Skumanich, A. 1997c, Nature, 389, 47

Westendorp Plaza, C., del Toro Iniesta J. C., Ruiz Cobo, B., Martínez Pillet, V., Lites B. W., & Skumanich, A. 1998, ApJ, 494 (in press)

Wood K. & Fox G.K. 1995, Inverse Problems, 11, 795

This manuscript was prepared with the AAS LaTeX macros v4.0.

FIGURE CAPTIONS

Fig. 1.— Three steps in the inversion procedure. From a constant-temperature atmosphere (a, dotted lines) resulting in no spectral lines, to the final step (c, solid lines) where the line profiles are well reproduced. Nine of the 40 lines employed for the inversion are displayed; *upper panel* (left to right): Fe I $\lambda\lambda$ 6082, 6151, 6173, and 6200 Å; *lower panel*: Ca I $\lambda\lambda$ 6166, 6455, and 6499 Å, and Cr I $\lambda\lambda$ 4801 and 4964 Å.

Fig. 2.— A detailed example of a synthetic line profile emerging from the obtained model atmosphere (solid line) compared to the solar observations (circles). The reproduction of the Ca I λ 6500 Å observed profile is excellent. The goodness of the fit is limited by the line asymmetries originating from convective motions.

Fig. 3.— Comparison between the solar photospheric temperature structure obtained using the inversion method (labeled MISS) and other classical solar models. MISS tends to be cooler in the outer layers and hotter in the inner ones.

Fig. 4.— Comparison between the continuum limb-darkening observed and predicted by different models in the optical spectral region. The model HSRA, empirically built from continuum observations, follows the observations very closely at all wavelengths while the model from the inversion of line profiles reproduces the limb darkening acceptably.

Fig. 5.— The center-to-limb variations of the equivalent widths (normalized to their value at the disk center) of three lines employed in the flux inversion and measured by Balthasar (1988) are closer to the MISS predictions than to any other model in this comparison.

Fig. 6.— Comparison between the solar flux measurements of Neckel & Labs (1984; filled triangles) and the pseudo-continuum estimated by Kurucz et al. (1984; dots), and the true continua predicted by different models. The pseudo-continuum of Kurucz et al. establishes

a lower limit to the true continuum, which is well-satisfied by three of the models considered: MISS, Kurucz, and HOLMU.

Fig. 7.— *Upper panel*: the observed profile (solid line) of the Ca I λ 6162 Å line, whose wings (enhanced in the graph) were included in the inversion, is nicely reproduced by the resulting model. There is also a good agreement with the other surrounding lines, which were not included in the inversion and without accurate oscillator strengths. *Lower panel*: a very good agreement is also found for the wings of the Na I D lines (not included in the inversion). For both the Na I D and Ca I $4s4p - 4s5s$ lines, accurate damping constants available from empirical measurements and/or theoretical estimates exist in the literature and have been used in the synthesis.

Fig. 8.— The meteoritic iron abundance and the laboratory transition probabilities measured by O'Brian et al. (1991) give an independent test for the reliability of the MISS model. Displayed are three neutral iron lines with clean profiles (following Meylan et al. 1993), not included in the inversion line sample: $\lambda\lambda$ 4635.85, 6027.05, and 6481.87 Å. The observed profiles are marked as dots while the other line styles are the same as in Fig. 3.

Table 1. Spectral lines used in the inversion.

Element	Wavelength (Å)	Exc. Pot. (eV)	$\log gf$	Element	Wavelength (Å)	Exc. Pot. (eV)	$\log gf$
Ca I	4578.557	2.52	–0.697	Ti I	5922.115	1.05	–1.410
Ca I	5512.986	2.93	–0.447	Ti I	6092.799	1.89	–1.323
Ca I	6161.297	2.52	–1.266	Ti I	6258.109	1.44	–0.299
Ca I	6162.183	1.89	–0.097	Ti I	6303.762	1.44	–1.510
Ca I	6166.441	2.52	–1.142	Ti I	6312.244	1.46	–1.496
Ca I	6455.604	2.52	–1.290	Ti I	7357.735	1.44	–1.066
Ca I	6499.656	2.52	–0.818	Fe I	4602.006	1.61	–3.150
Cr I	4801.028	3.12	–0.131	Fe I	5225.533	0.11	–4.790
Cr I	4964.931	0.94	–2.527	Fe I	5247.057	0.09	–4.950
Cr I	5272.002	3.45	–0.422	Fe I	5916.254	2.45	–2.990
Cr I	5300.751	0.98	–2.129	Fe I	5956.700	0.86	–4.610
Cr I	5312.859	3.45	–0.562	Fe I	6082.715	2.22	–3.570
Cr I	5787.922	3.32	–0.083	Fe I	6151.623	2.18	–3.300
Cr I	7355.899	2.89	–0.285	Fe I	6173.342	2.22	–2.880
Ti I	4758.122	2.25	0.481	Fe I	6200.321	2.61	–2.440
Ti I	4759.274	2.25	0.570	Fe I	6297.801	2.22	–2.740
Ti I	5113.445	1.44	–0.727	Fe I	6481.878	2.28	–2.980
Ti I	5295.781	1.05	–1.577	Fe I	6498.945	0.96	–4.700
Ti I	5490.154	1.46	–0.877	Fe I	6750.161	2.42	–2.620
Ti I	5866.457	1.07	–0.784	Fe I	6978.861	2.48	–2.500

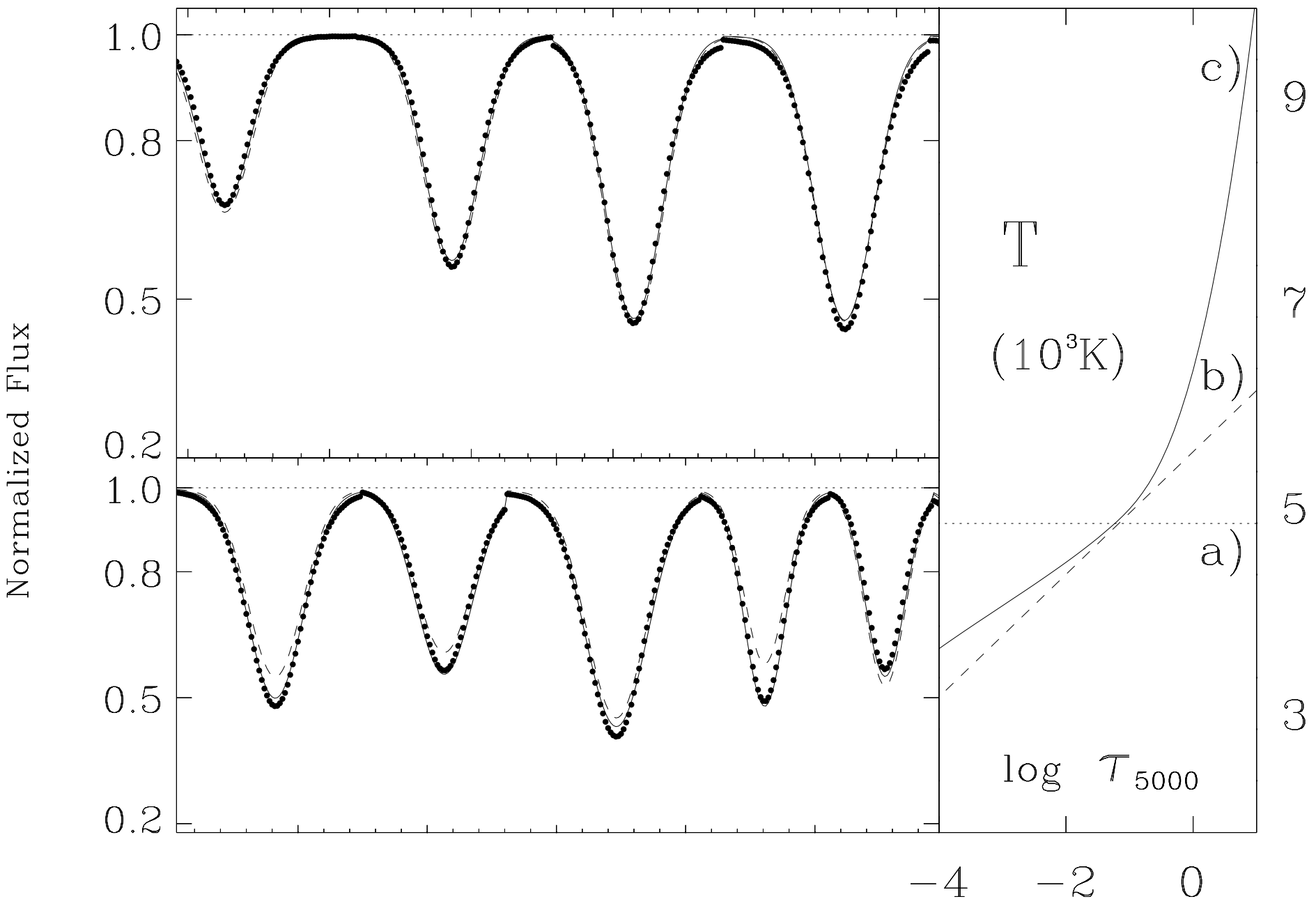
Normalized Flux
1.0
0.8
0.5
0.2
1.0
0.8
0.5
0.2
c)
b)
a)
T
(10³K)
9
7
5
3
log τ5000
−4
−2
0

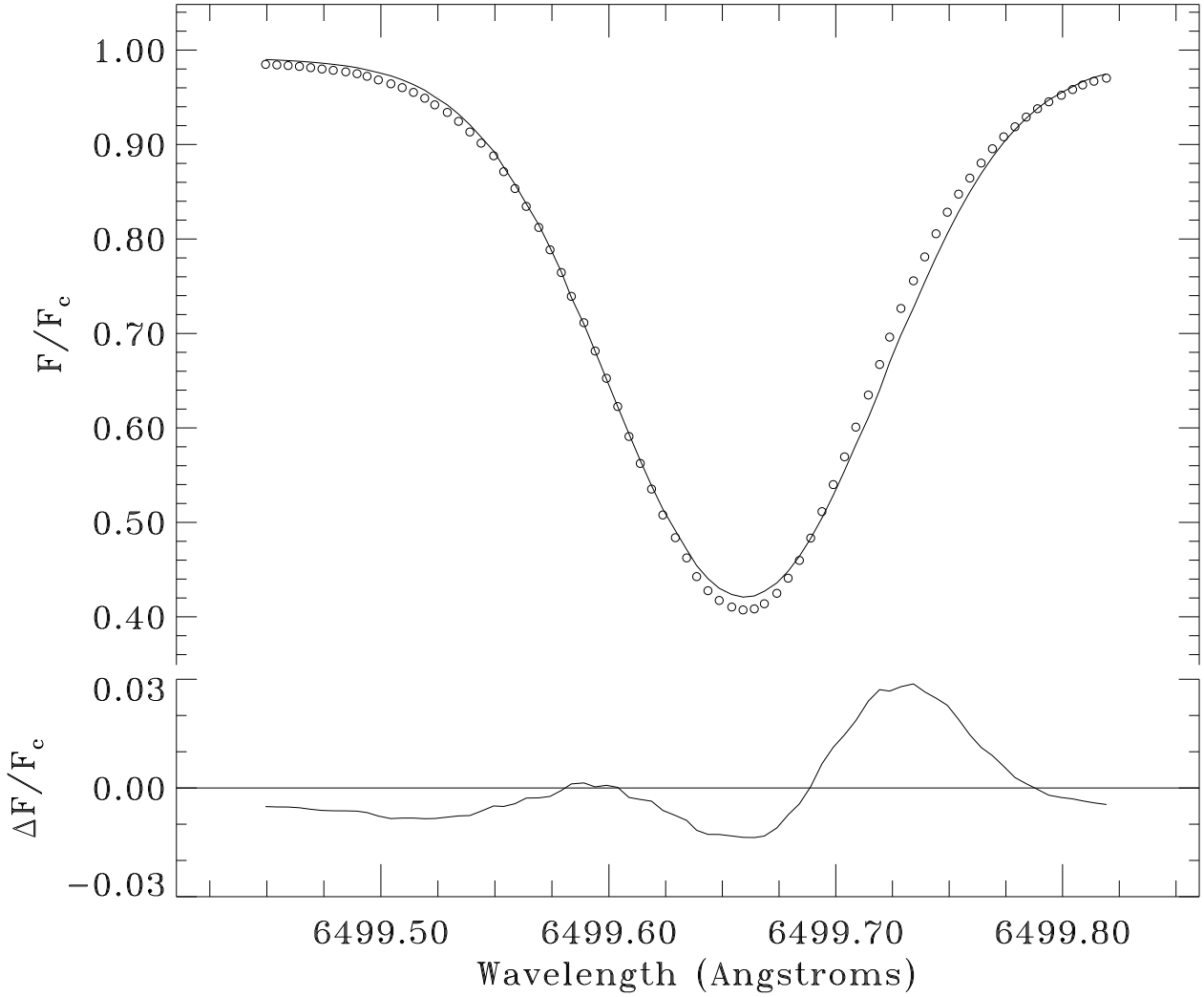
1.00
0.90
0.80
0.70
0.60
0.50
0.40
F/F_c
0.03
0.00
−0.03
ΔF/F_c
6499.50
6499.60
6499.70
6499.80
Wavelength (Angstroms)

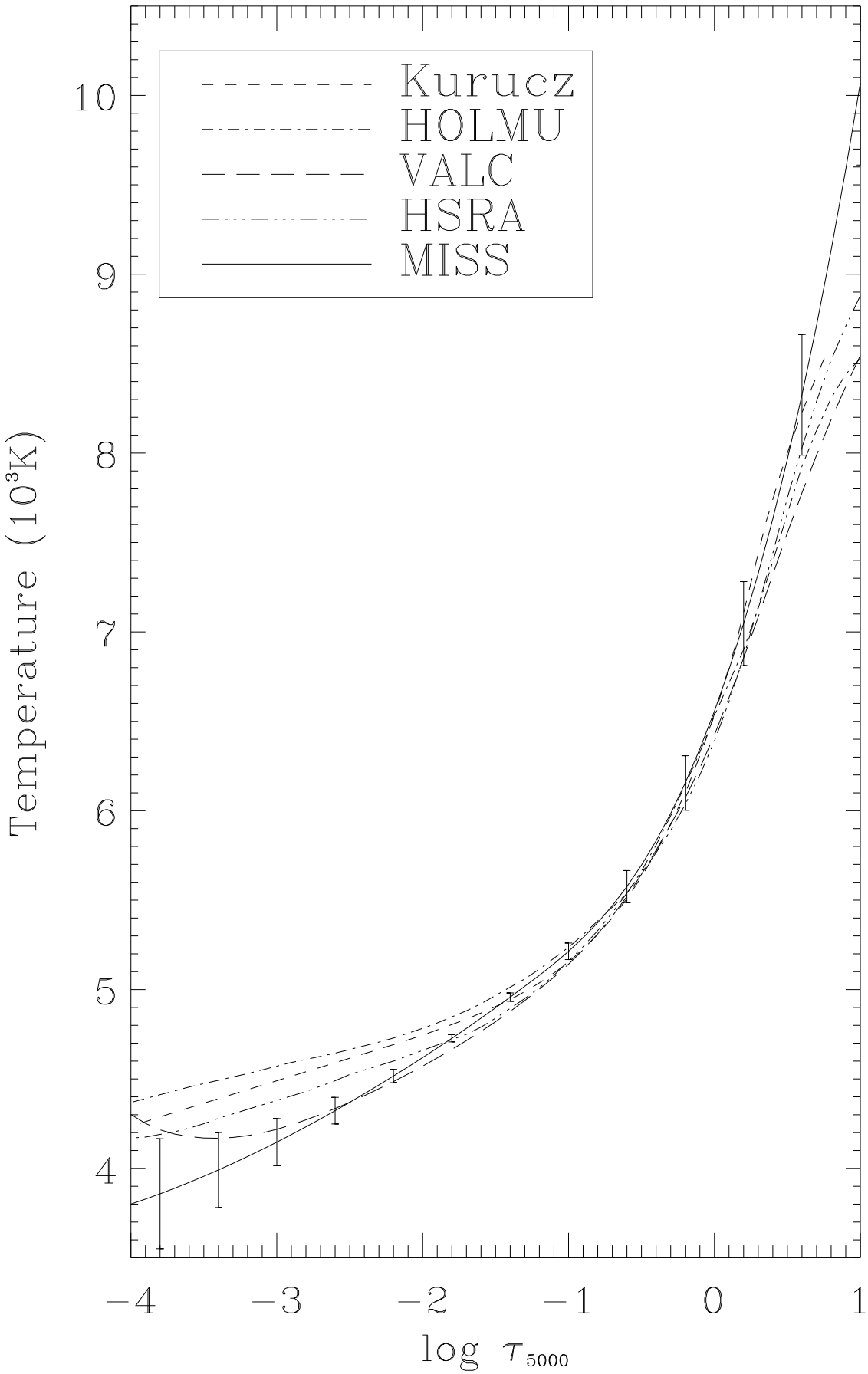
Kurucz
HOLMU
VALC
HSRA
MISS
Temperature (10^3K)
10
9
8
7
6
5
4
−4
−3
−2
−1
0
1
log τ_{5000}

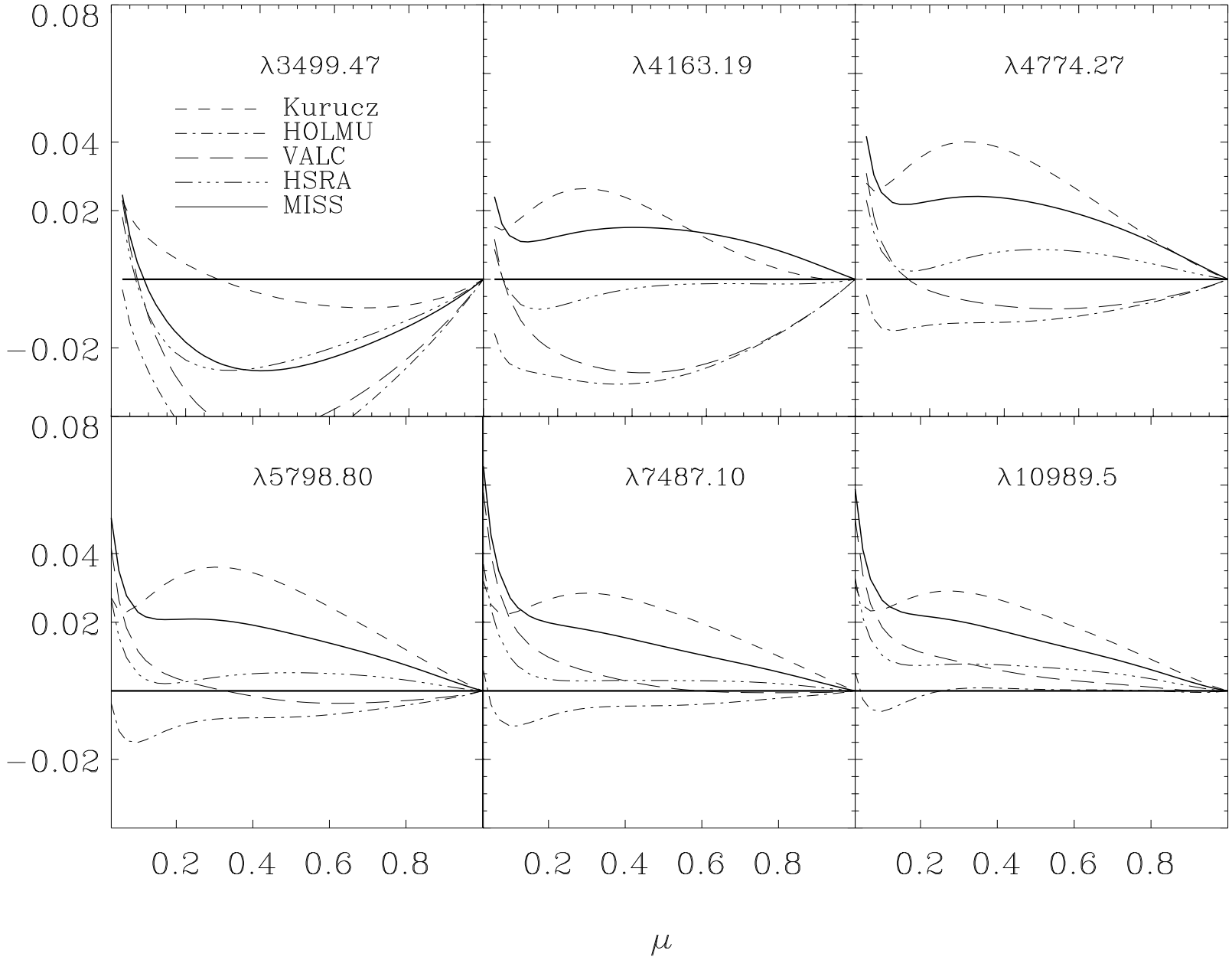
λ3499.47
λ4163.19
λ4774.27
λ5798.80
λ7487.10
λ10989.5
Kurucz
HOLMU
VALC
HSRA
MISS
0.08
0.04
0.02
−0.02
0.2
0.4
0.6
0.8
μ
$I^{obs}(\mu)/I^{obs}(1.0) - I^{syn}(\mu)/I^{syn}(1.0)$

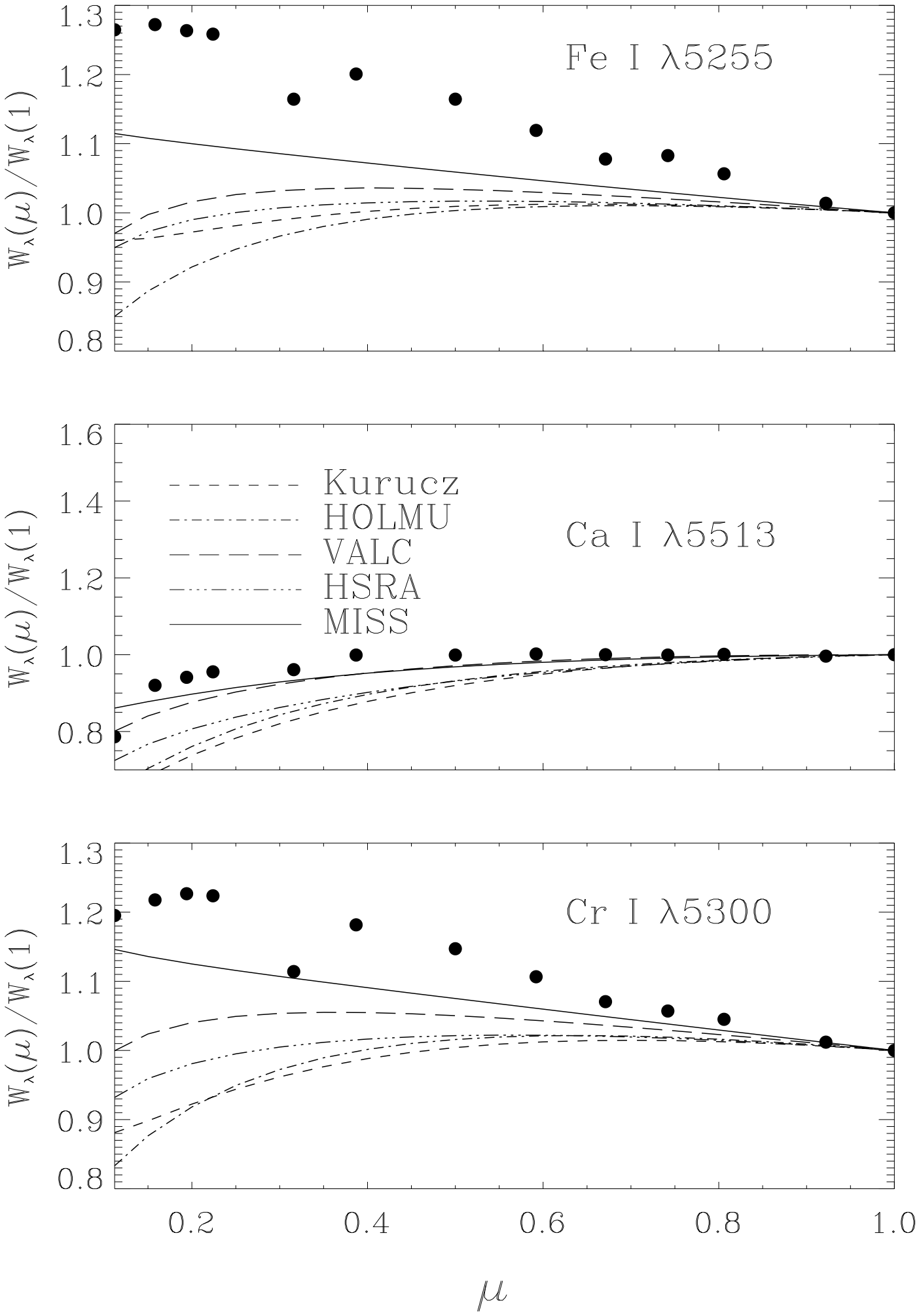
Fe I λ5255
Ca I λ5513
Cr I λ5300
Kurucz
HOLMU
VALC
HSRA
MISS
$W_\lambda(\mu)/W_\lambda(1)$
μ
0.2
0.4
0.6
0.8
1.0
0.8
0.9
1.0
1.1
1.2
1.3
1.4
1.6

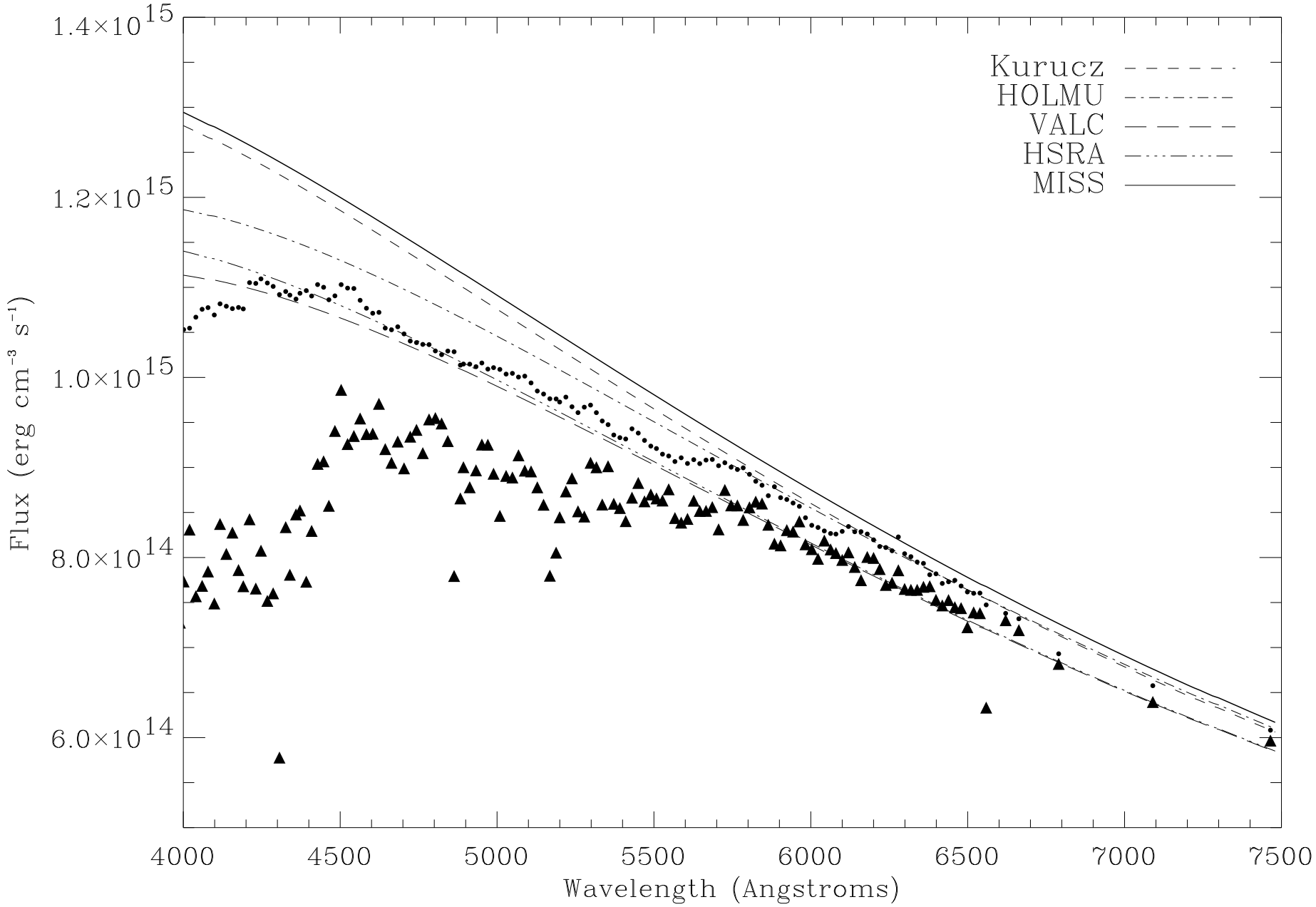
Kurucz
HOLMU
VALC
HSRA
MISS
1.4×10^15
1.2×10^15
1.0×10^15
8.0×10^14
6.0×10^14
Flux (erg cm^-3 s^-1)
4000
4500
5000
5500
6000
6500
7000
7500
Wavelength (Angstroms)

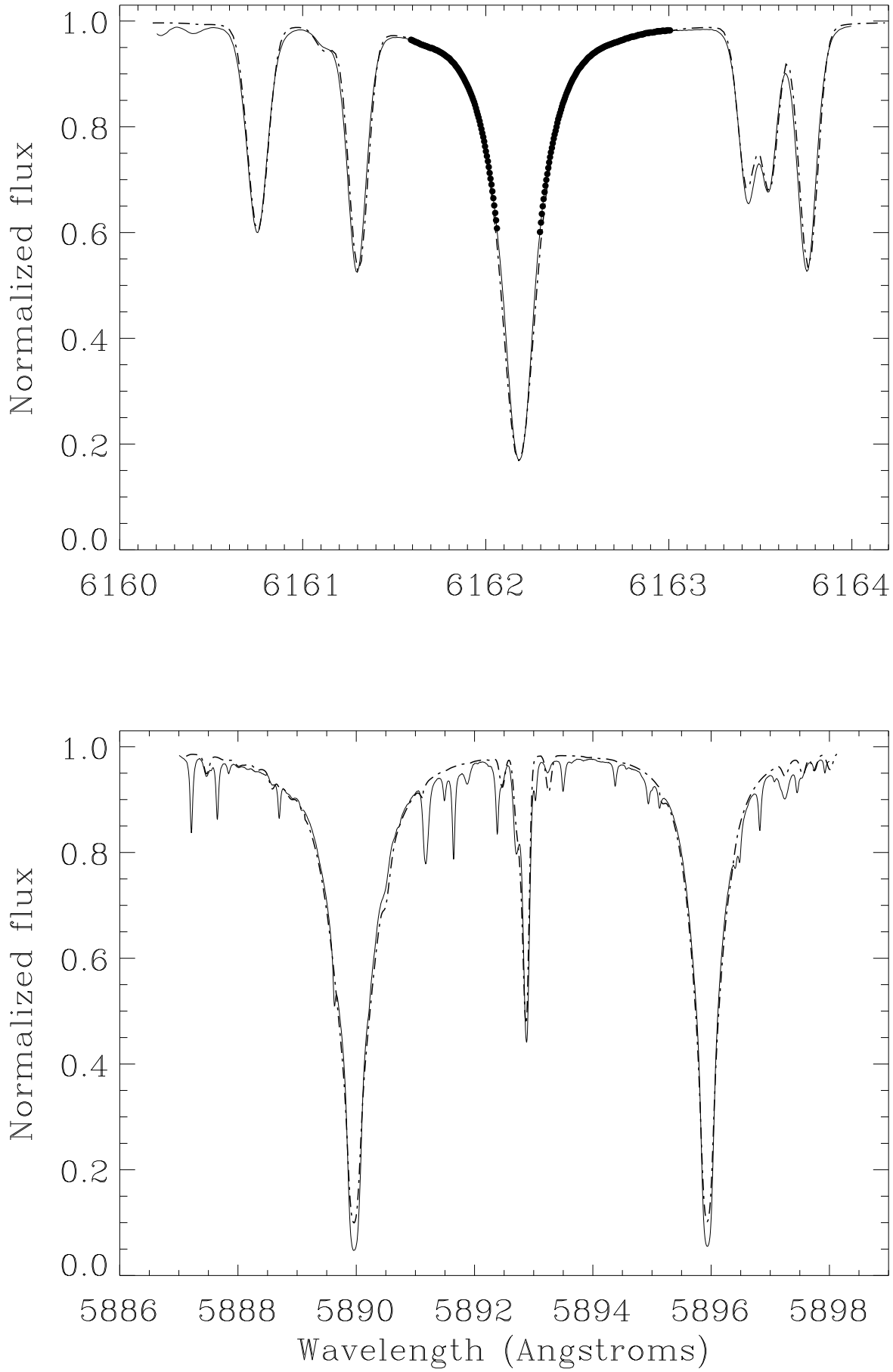
Normalized flux
1.0
0.8
0.6
0.4
0.2
0.0
6160
6161
6162
6163
6164
Normalized flux
1.0
0.8
0.6
0.4
0.2
0.0
5886
5888
5890
5892
5894
5896
5898
Wavelength (Angstroms)

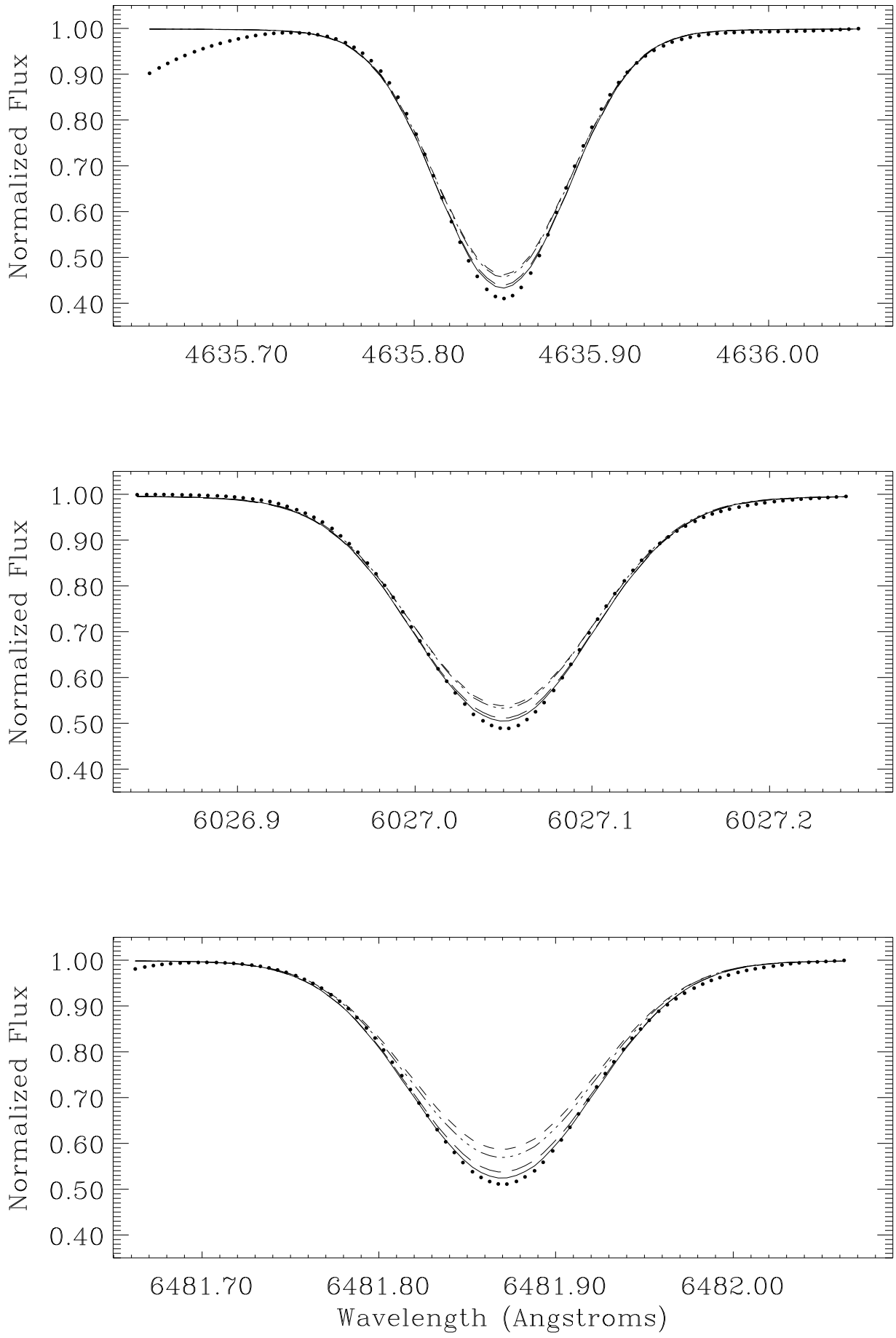
Normalized Flux
1.00
0.90
0.80
0.70
0.60
0.50
0.40
4635.70
4635.80
4635.90
4636.00
Normalized Flux
1.00
0.90
0.80
0.70
0.60
0.50
0.40
6026.9
6027.0
6027.1
6027.2
Normalized Flux
1.00
0.90
0.80
0.70
0.60
0.50
0.40
6481.70
6481.80
6481.90
6482.00
Wavelength (Angstroms)